

Collisional and thermal dissociation of J/ψ and Υ states at the LHC

Samuel Aronson^{1,*} Evan Borrás^{1,†} Brunel Odegard^{1,‡} Rishi Sharma^{2,§} and Ivan Vitev^{3,¶}
¹ *University of California, Santa Barbara, College of Creative Studies, Isla Vista, CA 93106, USA*
² *Tata Institute of Fundamental Research, Mumbai, Maharashtra 400005, India and*
³ *Los Alamos National Laboratory, Theoretical Division, Los Alamos, NM 87545, USA*

We present new results for the suppression of high transverse momentum charmonium [$J/\psi, \psi(2S)$] and bottomonium [$\Upsilon(1S), \Upsilon(2S), \Upsilon(3S)$] states in Pb+Pb collisions at the Large Hadron Collider. Our theoretical formalism combines the collisional dissociation of quarkonia, as they propagate in the quark-gluon plasma, with the thermal wavefunction effects due to the screening of the $Q\bar{Q}$ attractive potential in the medium. We find that a good description of the relative suppression of the ground and higher excited quarkonium states, transverse momentum and centrality distributions is achieved, when comparison to measurements at a center-of-mass energy of 2.76 TeV is performed. Theoretical predictions for the highest Pb+Pb center-of-mass energy of 5.02 TeV at the LHC, where new experimental results are being finalized, are also presented.

PACS numbers:

I. INTRODUCTION

The fate of quarkonia – for example the J/ψ and the Υ meson families – in a thermal medium, such as the quark-gluon plasma (QGP) created in heavy ion collisions (HIC), can help us characterize its properties. In particular, quarkonia are sensitive to the space-time temperature profile and transport coefficients of the QGP, see [1–3] for recent reviews. Experimentally, a key observable that carries such information is the nuclear modification factor of the yields of quarkonia in nucleus-nucleus (AA) collisions, when compared to their yields in nucleon-nucleon (NN) collisions scaled with the number of binary interactions

$$R_{AA} = \frac{1}{\langle N_{\text{coll.}} \rangle} \frac{d\sigma_{AA}^{\text{Quarkonia}}/dydp_T}{d\sigma_{pp}^{\text{Quarkonia}}/dydp_T} \quad (1)$$

In HICs one expects that the short distance formation dynamics of a $Q\bar{Q}$ pair is not affected since $m_Q \gg T$ where T is the typical temperature of the QGP. To simplify the calculations, it is often also assumed that the matrix elements for transition of $Q\bar{Q}$ to quarkonia is not modified, and for every binary collision the formation of a specific quarkonium state happens with the same

probabilities as in NN collisions. This takes a time scale close to its inverse of its binding energy. However, due to the screening of the color interaction between Q and \bar{Q} in a deconfined QGP [4], as well as processes leading to the dissociation [5] of quarkonium states, we expect the yields of quarkonia to be suppressed in heavy ion collisions ($R_{AA} < 1$).

Several methods have been used to estimate screening and dissociation effects encountered by a quarkonium in a thermal medium. A widely used approach is based on the intuitive idea that the real part of the “finite temperature potential” between two (nearly) static heavy quarks captures the screened $Q\bar{Q}$ interaction while the imaginary part of the potential captures quarkonium dissociation. For $T = 0$, the real part can be quantitatively obtained by calculating the Polyakov loop correlation functions [6–8]. For $T > 0$, the connection between various correlators calculated on the lattice and the potential between Q and \bar{Q} is subtle [6–9]. While the singlet free energy $F_1(r)$ of the $Q\bar{Q}$ state as a function of the separation r , and internal energy $U(r)$ can be extracted from the lattice data, the connection of either of the two with the $Q\bar{Q}$ potential is indirect. An important step in clarifying this connection was taken in Ref. [10], which showed that the “potential” between two heavy quarks is complex, with the imaginary part connected to thermal processes that can lead to dissociation of quarkonia. Significant progress has been made in the perturbative calculation of the real and imaginary part of the $Q\bar{Q}$ potential for $Q\bar{Q}$ at rest in the medium [10–12] or moving slowly in the medium [13]. Analytic calculations can be performed in certain regimes by considering various hierarchies of energy scales. For

*Electronic address: samuelaronson@umail.ucsb.edu

†Electronic address: evanborras@umail.ucsb.edu

‡Electronic address: bodegard@umail.ucsb.edu

§Electronic address: rishi@theory.tifr.res.in

¶Electronic address: ivitev@lanl.gov

example, one has to assume that T and m_Q are large enough so that perturbation theory is valid all the way down to energy scales πT and the binding energy E_b .

While the real part of the potential for $T \gg \Lambda_{QCD}$ can be obtained using perturbation theory, non-perturbative effects are substantial near the crossover temperature and it is better to estimate this quantity from lattice calculations by matching the Euclidean correlators measured on the lattice [8, 9, 14, 15] with those evaluated using the potential. The extraction of the imaginary part of the potential using this technique is challenging and often perturbative estimates are used. Extensive phenomenological study of quarkonium suppression by using this approach has been performed [16–19]. Recently, approaches treating the $Q\bar{Q}$ as an open quantum system were developed, where a stochastic equation is written for the evolution of the $Q\bar{Q}$ wavefunction [20–23]. We also note that the connection between the heavy quark correlators measured on the lattice and in a non-perturbative framework using the in medium T-matrix has been made in Refs. [24, 25]. Quarkonium suppression [26–28], as well as low p_T observables like heavy quark flow have been studied using this approach. Thermal properties of quarkonia have also been investigated in the strong coupling regime using AdS/CFT techniques, see Ref. [29].

In this paper we calculate the differential R_{AA} as a function of p_T by solving rate equations [30–32] describing the change in the yields as a function of time in HICs. Conceptually, our approach resembles treating the $Q\bar{Q}$ as an open quantum system. It was, however, introduced earlier to describe the attenuation of open heavy flavor [30]. Gluon exchanges with the medium lead to the modification of the $Q\bar{Q}$ state and, hence, a reduction in the overlap with the quarkonium wavefunction. However we do not connect the imaginary part of the potential calculated in approaches cited above to the decay rate. This is because we focus on R_{AA} at high p_T . For high p_T partons traversing the medium, a very successful picture is that the interactions with the medium lead to transverse momentum broadening. The decay rate in our calculation is related to the accumulation of relative momenta between Q and \bar{Q} .

The form of the rate equations is the same as used in our previous work [32] and they involve the dissociation time and the formation time as inputs. The formation time in our formalism is a measure of the time scale on which the proto-quarkonium $Q\bar{Q}$ state develops interactions with the medium and its overlap with the quarkonia becomes substantial. We vary it in the neighborhood of $\mathcal{O}(1 \text{ fm})$. The dissociation time scale is computed as in [32] by calculating the survival probability of the quarkonia.

One conceptual change in our framework, when compared to [32], is that we use the real part of the lattice motivated thermal potentials [7, 9, 14] to solve for the quarkonium wavefunction and square the overlap with the thermal wavefunction to get the survival probability. This is justified if the time scales on which the medium

screens the $Q\bar{Q}$ interaction is smaller than the formation time as well as the dissociation time. A rough estimate of the Debye screening time is the inverse of the Debye screening mass (μ_D), which is $\sim gT$. For $g = 1.85$, $(1/\mu_D)$ is numerically smaller than $1/2 \text{ fm}$ for most of the evolution of the medium at the LHC. On the other hand, the formation is taken to be $\sim 1 \text{ fm}$. Finally, this puts a constraint that the minimum dissociation time consistent within our formalism is roughly 1 fm . We see that while there is no substantial hierarchy between $1/\mu_D$ and the formation and dissociation time scales in our calculation, numerically $1/\mu_D$ is smaller and, hence, we work in this approximation.

In addition, we make two technical improvements. First, we consider a $2 + 1$ dimensional viscous hydrodynamic medium, rather than a simplified $1 + 1$ dimensional Bjorken expansion, as a model for the QGP [33]. An important element of our approach is the use of non-relativistic QCD (NRQCD) [34] to obtain the baseline nucleon-nucleon cross sections for quarkonia and understand the p_T -dependent feed down. The second technical improvement is a refit of the long distance matrix elements for χ_c and $\psi(2S)$ to obtain a better description of the high p_T part of their differential spectra. We are further motivated by the fact that new experimental results that extend the measurements of quarkonia to high p_T have appeared. Improved measurements of the higher excited states, such as the $\psi(2S)$ and the $\Upsilon(2S)$ and $\Upsilon(3S)$, that are differential in transverse momentum are particularly useful in constraining the mechanisms of quarkonium suppression.

In this paper we focus on the nuclear modification of the prompt J/ψ and Υ states around mid-rapidity at the LHC and at high transverse momentum [35–40]. In section II we describe the theoretical model that is employed in the calculation of quarkonium production in heavy ion collisions. Phenomenological results for the nuclear modification of the J/ψ and Υ states are presented in section III. Our conclusions and outlook are given in section IV.

II. THEORETICAL FORMALISM

Quarkonia are bound states of heavy quarks (Q) and antiquarks (\bar{Q}), and a concrete picture of the dynamics of the heavy quark pair ($Q\bar{Q}$) in NN collisions is given by non-relativistic quantum chromodynamics (NRQCD) [34]. In this effective theory, the initial hard collision produces a short distance ($\sim 1/m_Q$) $Q\bar{Q}$ pair in a color-singlet or an octet state with a specific spin and orbital structure. The production cross-section for this short-distance state can be calculated using perturbative QCD. This $Q\bar{Q}$ state evolves into a quarkonium state with probabilities that are given by long distance matrix elements (LDMEs). For color-octet states, this evolution process also involves the emission of soft partons to form a net color-singlet object which we assume occurs on a

time scale which is shorter than $\mathcal{O}(1\text{ fm})$.

This framework has been successfully used to calculate the unpolarized differential yields of quarkonia versus the transverse momentum (p_T) in proton-proton (pp) or proton-antiproton ($p\bar{p}$) collisions [41–44]. An accurate description of both the cross sections and polarization of quarkonia in hadronic reactions still remains a challenge [45]. Recently, it has been suggested [46–48] that new experimental measurements of quarkonium production inside jets [49] may help better constrain the relevant LDMEs. The focus of this paper is, however, different. Our study concentrates on the production, propagation, and dissociation of quarkonium states in strongly interacting matter. We follow the NRQCD calculation outlined in [32] and use the LDMEs extracted there to give good description of the cross sections for bottomonia for pp and $p\bar{p}$ collisions for p_T in the range of 5 to 30 GeV. For charmonia we improve the χ_c fitting procedure by allowing the singlet matrix element as a free parameter. We also refit LDMEs for the $\psi(2S)$ by fitting the LHC 7 TeV and CDF 1.8 TeV data. Both these changes make the spectra for χ_c and $\psi(2S)$ in the $p_T \sim 10 - 20$ GeV region softer and improve the description of data without spoiling the agreement at lower p_T .

In order to address quarkonium attenuation in heavy ion reactions, we need to understand the J/ψ and Υ states' behavior and melting at finite temperature in the QGP, and the dissociation processes due to collisional interactions with the quasi-particles of the QCD medium. To accomplish this, a detailed knowledge of the wavefunctions at zero and finite temperatures is necessary. We start by solving the Schrödinger equation by separating the radial and angular parts of the wavefunction, $\psi(\mathbf{r}) = Y_l^m(\hat{r})R_{nl}(r)$. The reduced equation for the radial part can be written as

$$\left[-\frac{1}{2\mu_{\text{red}}} \frac{\partial^2}{\partial r^2} + \frac{l(l+1)}{2\mu_{\text{red}}r^2} + V(r) \right] rR_{nl}(r) = (E_{nl})rR_{nl}(r), \quad (2)$$

where $\mu_{\text{red}} = \frac{m_Q}{2}$ is the reduced mass, and n and l are the principal and orbital quantum numbers, respectively. $V(r)$ is the potential between the two heavy quarks, which can be estimated from the lattice [7]. The binding energy of the meson is then $E_{nl}^b = V(\infty) - E_{nl}$. For $T = 0$ we take the form of the potential to be of the standard Cornell form

$$V(r) = -\frac{\xi}{r} + \sigma r, \quad \xi = 0.385, \quad \sigma = 0.224 \text{ GeV}^2. \quad (3)$$

The form of the potential has been validated in multiple lattice calculations by evaluating the Polyakov loop correlator as a function of the quark-antiquark separation. The Cornell long-distance part is cut off at $r_{\text{max}} = 1.1$ GeV [9] to model string breaking on this length scale. This defines the value of $V(\infty) \approx 1.2$ GeV. For the mass of the heavy quark we take $m_c = 1.34$ for the charm quark and $m_b = 4.5$ for the bottom quark. For

$T > 0$ the form of the real part of the potential we use is the internal energy found in [6]. We have checked that the potentials we use are quite close to the internal energies computed in the more recent work [7] and the potentials used in [14]. Internal energies provide a stronger binding potential compared to the single free energies [7]. The use of the internal energies can be justified if the dynamics of the quarkonia are too rapid for the $Q\bar{Q}$ potential to fully thermalize, which might be especially likely for high p_T quarkonia in the medium. With this setup, solutions are obtained for a variety of temperatures and for the S-wave and P-wave states. Even though we are primarily interested in the J/ψ , $\psi(2S)$, and $\Upsilon(nS)$, the P-wave χ_c and χ_b contribute via feed down.

l	n	E_{nl}^b (GeV)	$\sqrt{\langle r^2 \rangle}$ (GeV $^{-1}$)	k^2 (GeV 2)	Meson
0	1	0.700	2.24	0.30	J/ψ
0	2	0.086	5.39	0.05	$\psi(2S)$
1	1	0.268	3.50	0.20	χ_c
0	1	1.122	1.23	0.99	$\Upsilon(1S)$
0	2	0.578	2.60	0.22	$\Upsilon(2S)$
0	3	0.214	3.89	0.10	$\Upsilon(3S)$
1	1	0.710	2.07	0.58	$\chi_b(1P)$
1	2	0.325	3.31	0.23	$\chi_b(2P)$
1	3	0.051	5.57	0.08	$\chi_b(3P)$

TABLE I: Charmonia and bottomonia wavefunctions at zero temperature. l refers to the angular momentum of the $Q\bar{Q}$ state, while n is the radial quantum number. E_{nl}^b is the binding energy, $\sqrt{\langle r^2 \rangle}$ is the root mean square (RMS) radius of the quarkonium state, and k^2 is the mean square momentum.

l	n	E_{nl}^b (GeV)	$\sqrt{\langle r^2 \rangle}$ (GeV $^{-1}$)	k^2 (GeV 2)	Meson
0	1	0.366	2.34	0.27	J/ψ
0	2	-	-	-	$\psi(2S)$
1	1	0.003	8.15	0.04	χ_c
0	1	0.782	1.23	0.98	$\Upsilon(1S)$
0	2	0.244	2.72	0.20	$\Upsilon(2S)$
0	3	-	-	-	$\Upsilon(3S)$
1	1	0.371	2.09	0.57	$\chi_b(1P)$
1	2	0.040	4.56	0.12	$\chi_b(2P)$
1	3	-	-	-	$\chi_b(3P)$

TABLE II: Charmonia and bottomonia wavefunctions at finite temperature. We chose a temperature of 192 MeV to illustrate the disappearance of the weakly bound states and the changes in the quarkonium wavefunctions.

Pertinent results for the quarkonium and bottomonium wavefunctions are presented in Table I and Table II for zero temperature (T) and $T = 192$ MeV, respectively. We show the binding energy E_{nl}^b and the root mean square (RMS) size $\sqrt{\langle r^2 \rangle}$ of the quarkonium state. The RMS size changes only slowly with T , except near the dissociation temperature. We have chosen the finite temperature value ~ 190 MeV to illustrate that several states, i.e. $\psi(2S)$, $\Upsilon(3S)$, and $\chi_b(3P)$, cease to exist even with our selected strong binding potential. The χ_c and $\chi_b(2P)$ states are very near dissociation. If we Fourier transform

to momentum space, the mean squared momentum k^2 can also be evaluated and is given in Tables I and II. We note that while there is a correlation between the width of the wavefunctions of quarkonia and their binding energies, this correlation is highly non-linear. The widths change rapidly only near dissociation when $E_{nl}^b \rightarrow 0$.

In this work we are interested in large transverse momentum quarkonia and it is convenient to work in light cone momenta and with light-cone wavefunctions. The relation between the instant form and the light-cone form of the momentum space wavefunctions for mesons was discussed in detail in [31, 32]. For the case of quarkonia, the color-singlet contribution can be understood as one matching to the lowest order ($n = 2$) Fock component of the state. A color-octet initial state must emit at least one gluon for a color neutral hadron to be produced. In either case the heavy meson or proto-quarkonium state of momentum $\vec{P}^+ = (P^+, \mathbf{P})$ can be approximated as:

$$|\vec{P}^+\rangle = \int \frac{d^2\mathbf{k}}{(2\pi)^3} \frac{dx}{2\sqrt{x(1-x)}} \frac{\delta_{c_1 c_2}}{\sqrt{3}} \psi(x, \mathbf{k}) \times a_Q^\dagger c_1(x\vec{P}^+ + \mathbf{k}) b_Q^\dagger c_2((1-x)\vec{P}^+ - \mathbf{k}) |0\rangle, \quad (4)$$

where a^\dagger (b^\dagger) represent an “effective” heavy quark (antiquark) in the 3 ($\bar{3}$) state, c_1, c_2 being the color indices [31, 32]. The light cone wavefunction $\psi(x, \mathbf{k})$ in Eq. (4), which describe the longitudinal momentum fraction x ($1-x$) distribution and the transverse momentum \mathbf{k} ($-\mathbf{k}$) distribution of heavy quarks (antiquarks) is given by

$$\psi(x, \mathbf{k}) = \text{Norm} \times \exp\left(-\frac{\mathbf{k}^2 + m_Q^2}{2\Lambda^2(T)x(1-x)}\right), \quad \frac{1}{2(2\pi)^3} \int dx d^2\mathbf{k} |\psi(x, \mathbf{k})|^2 = 1. \quad (5)$$

In Eq. (5) $\Lambda(T)$ is the transverse momentum width of the light-cone wavefunction which needs to be constrained at 0 and finite temperature to the mean transverse momentum squared from the solution to the Schrödinger equation, which remains invariant under boost. If we introduce the notation $\Delta\mathbf{k} = \mathbf{k}_1 - \mathbf{k}_2 = 2\mathbf{k}$, the equation for $\Lambda(T)$ reads

$$\frac{1}{2(2\pi)^3} \int dx d^2\mathbf{k} \Delta\mathbf{k}^2 |\psi(x, \mathbf{k})|^2 = 4\langle\mathbf{k}^2\rangle = \frac{2}{3}\kappa^2. \quad (6)$$

The factor 2/3 comes from the 2D projection of the mean squared transverse momentum κ^2 from the instant-form wavefunction.

The temperature and/or density profiles of the medium, which play an important role in the dissociation of quarkonia, can be obtained from hydrodynamic simulations of the QGP [33, 50, 51] in 2.76 TeV and 5.02 TeV Pb+Pb collisions at the LHC. Specifically, we use the iEBE-VISHNU (2+1)-dimensional event-by-event viscous hydrodynamic package [33]. A sample tem-

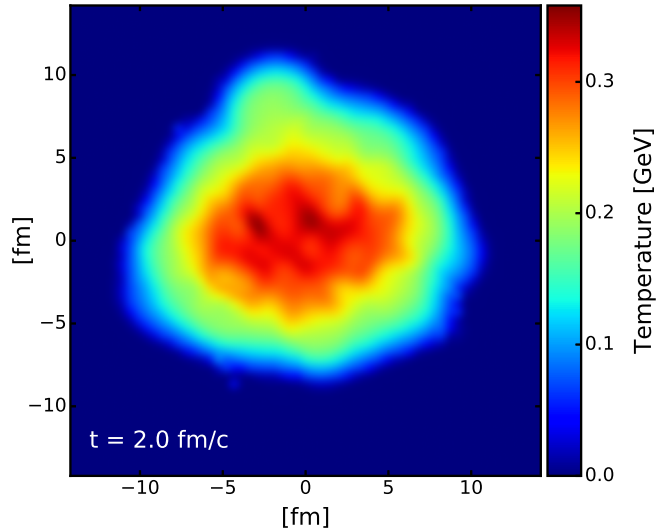


FIG. 1: (Color online) Example of the temperature profile of the QGP at a typical time $t = 2$ fm on 0-10% central Pb+Pb collisions at $\sqrt{s} = 2.76$ TeV the LHC. Glauber initial conditions and $\eta/s = 0.08$ are used in a 2+1D hydrodynamic simulation based on [33].

perature distribution at time $t = 2$ fm when the interplay between the formation and dissociation of quarkonia is important in setting the final observed J/ψ and Υ multiplicities is shown in Fig. 1. By comparing the temperature in the different points in the (x, y) plane perpendicular to the collision axis to the results in Table II one can get a sense of how the different quarkonium states will be attenuated in heavy ion collisions relative to proton collisions.

The propagation of a $Q\bar{Q}$ state in matter is accompanied by collisional interactions mediated at the partonic level, as long as the momentum exchanges between the medium quasi-particles and the heavy quarks can resolve the partonic structure of the meson. The related modification of the quarkonium wavefunction in Eq. (5) can lead to the dissociation of J/ψ s and Υ s in addition to the thermal effects. The cumulative one dimensional momentum transfer for a quarkonium state that starts at transverse position \mathbf{x}_0 and propagates with velocity β , such that $\mathbf{x}(\tau) = \mathbf{x}_0 + \beta(\tau - t_0)$, reads

$$\chi\mu_D^2\xi = \int_{t_0}^t d\tau \frac{\mu_D^2(\mathbf{x}(\tau), \tau)}{\lambda_q(\mathbf{x}(\tau), \tau)} \xi. \quad (7)$$

Here $\mu_D^2 = g^2 T^2 (1 + N_f/6)$ is the Debye screening scale and we use 2 active light quark flavors $N_f = 2$. The scattering inverse length of the quark is $1/\lambda_q = \sigma_{qq}\rho_q + \sigma_{qg}\rho_g$, where ρ_q and ρ_g are the partial densities of light quarks and gluons in the QGP. We label the cumulative one dimensional momentum transfer $\chi\mu_D^2\xi$ in analogy with a

uniform static medium where the Debye scale is fixed and $\chi = L/\lambda_q$ is the opacity. The elastic scattering cross sections are given by

$$\sigma_{qq} = \frac{1}{18\pi} \frac{g^4}{\mu_D^2}, \quad \sigma_{q\bar{q}} = \frac{1}{8\pi} \frac{g^4}{\mu_D^2}. \quad (8)$$

Last but not least, ξ is a parameter related to the heavy quark broadening from multiple scattering in the QGP [30, 52]. In the limit of strictly soft interactions $\xi = 1$ and an enhancement of $\xi \sim \text{few}$ may arise from the power law tails of the Moliere multiple scattering.

We initialize the wavefunction $\psi_i(\Delta\mathbf{k}, x)$ of the proto-quarkonium $Q\bar{Q}$ state with a width $\Lambda_0 \equiv \Lambda(T=0)$. This is a natural choice since in the absence of a medium it will evolve on the time-scale of $\mathcal{O}(1\text{fm})$ or greater into the observed heavy meson. By propagating in the medium this initial wavefunction accumulates transverse momentum broadening $\chi\mu_D^2\xi$. The probability that this $Q\bar{Q}$ configuration will transition into a final-state heavy meson with thermal wavefunction $\psi_f(\Delta\mathbf{k}, x)$ with $\Lambda(T)$ is given by

$$P_{f \leftarrow i}(\chi\mu_D^2\xi, T) = \left| \frac{1}{2(2\pi)^3} \int d^2\mathbf{k} dx \psi_f^*(\Delta\mathbf{k}, x) \psi_i(\Delta\mathbf{k}, x) \right|^2 \\ = \left| \frac{1}{2(2\pi)^3} \int dx \text{Norm}_f \text{Norm}_i \pi e^{-\frac{m_Q^2}{x(1-x)\Lambda(T)^2}} e^{-\frac{m_{\bar{Q}}^2}{x(1-x)\Lambda_0^2}} \right. \\ \left. \times \frac{2[x(1-x)\Lambda(T)^2][\chi\mu_D^2\xi + x(1-x)\Lambda_0^2]}{[x(1-x)\Lambda(T)^2] + [\chi\mu_D^2\xi + x(1-x)\Lambda_0^2]} \right|^2. \quad (9)$$

In Eq. (9) Norm_i is the normalization of the initial state, including the transverse momentum broadening from collisional interactions, and Norm_f is the normalization of the final state. The dissociation rate for the specific quarkonium state can then be expressed as

$$\frac{1}{t_{\text{diss.}}} = - \frac{1}{P_{f \leftarrow i}(\chi\mu_D^2\xi, T)} \frac{dP_{f \leftarrow i}(\chi\mu_D^2\xi, T)}{dt}. \quad (10)$$

It will enter the time evolution of the J/ψ s and Υ s in the medium. To visualize the dissociation rate, we present $1/\tau_{\text{diss.}}$ as a function of time in Fig. 2 for 0-10% central Pb+Pb collisions at the LHC at \sqrt{s} per nucleon pair of 2.76 TeV. We have weighed the dissociation rates with the binary collision density in the plane perpendicular to the collision axis and averaged over multiple hydrodynamic events. The top panel shows the dissociation rates of charmonium states and the bottom panel shows the corresponding rates for bottomonium state. We find that the modification of the ground states, such as J/ψ , $\Upsilon(1S)$ is dominated by dissociation at the early stages of the evolution of the QGP, whereas excited weakly bound states, such as are $\psi(2S)$, $\chi_b(3P)$, can be strongly modified until they escape the medium.

Finally, we note that effects that are suppressed at high transverse momentum, such as recombination [53] of unbound Q and \bar{Q} because of the Boltzmann suppression factor [54], the Cronin effect [55], and power

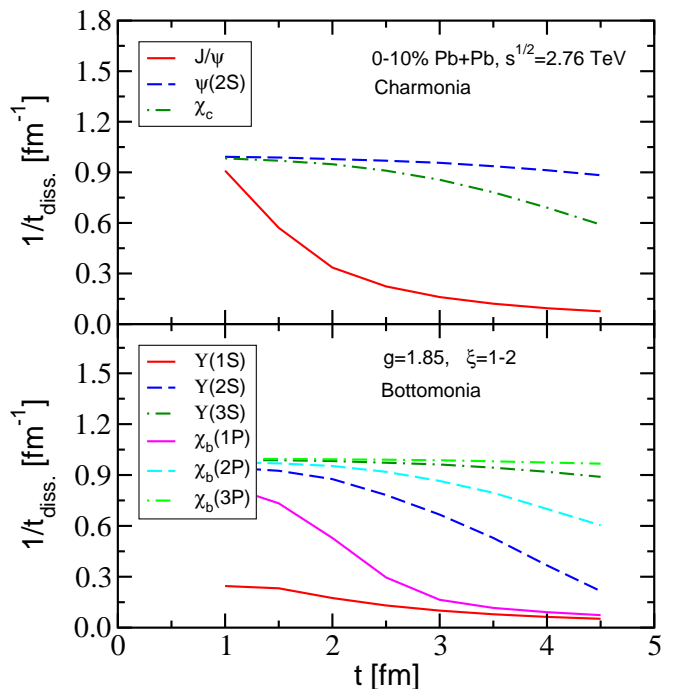


FIG. 2: (Color online) The dissociation rate $1/\tau_{\text{diss.}}$ for charmonium and bottomonium states in 0-10% central Pb+Pb collisions at $\sqrt{s} = 2.76$ TeV is shown in the top and bottom panels, respectively. We select the coupling between the quarks and the medium $g = 1.85$ and the broadening parameter $\xi = 1$.

corrections [56] do not play a role. Cold nuclear matter (CNM) energy loss might affect production cross sections [57], but its effects become significant at very high p_T near the kinematic threshold [58]. Last but not least, it was also found that leading-twist shadowing effects near mid-rapidity at high transverse momentum at the LHC are small [59]. While experimental results in p +Pb collisions at the LHC cannot exclude CNM effects at the 5 – 10% level at $p_T > 5$ GeV around mid-rapidity, they are also consistent with no nuclear modification [60–62]. For these reasons, for our study at $|y| < 2.4$, $p_T > 5$ GeV we neglect these effects.

III. PHENOMENOLOGICAL RESULTS

In this section we present the phenomenological results of our theoretical model for quarkonium dissociation due to thermal wavefunction effects and collisional breakup. For every centrality class and hydrodynamic event we distribute the production of the proto-quarkonium states according to the binary collision density in the 2D plane perpendicular to the collision axis. The azimuthal distribution in the directions of quarkonium propagation is uniform and we also average over multiple fluctuating hydrodynamic events that describe the QGP background.

For each quarkonium state the dynamics of production

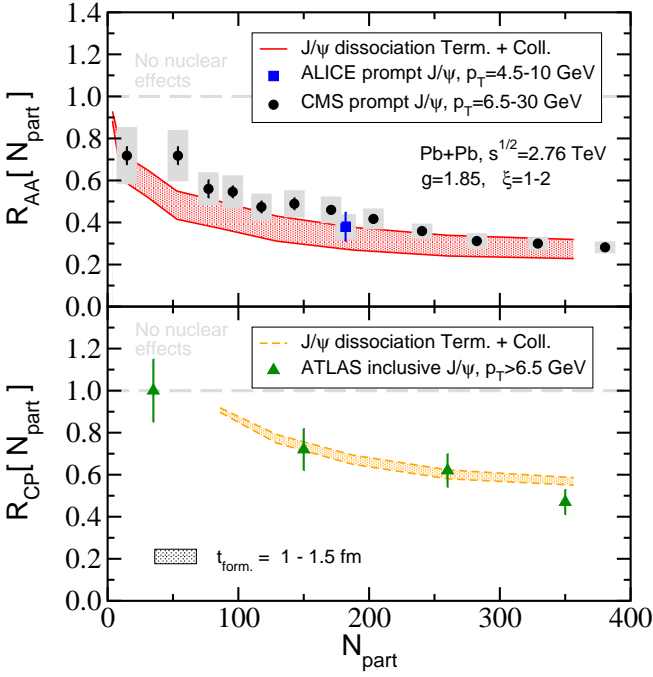


FIG. 3: (Color online) Comparison of theoretical results for prompt J/ψ suppression for $p_T > 6.5$ GeV to LHC Pb+Pb results at $\sqrt{s} = 2.76$ TeV. Top panel: N_{part} dependence versus ALICE [35] and CMS measurements [38]. Bottom panel: R_{CP} as a function of N_{part} versus ATLAS measurements [37].

and propagation through the QCD medium described above is given by a set of differential equations:

$$\frac{d}{dt} \left(\frac{d\sigma^{Q\bar{Q}}(t; p_T)}{dp_T} \right) = -\frac{1}{t_{\text{form.}}} \frac{d\sigma^{Q\bar{Q}}(p_T)}{dp_T}, \quad (11)$$

$$\frac{d}{dt} \left(\frac{d\sigma^{\text{meson}}(t; p_T)}{dp_T} \right) = \frac{1}{t_{\text{form.}}} \frac{d\sigma^{Q\bar{Q}}(t; p_T)}{dp_T} - \frac{1}{t_{\text{diss.}}} \frac{d\sigma^{\text{meson}}(t; p_T)}{dp_T}, \quad (12)$$

$$\frac{d}{dt} \left(\frac{d\sigma^{\text{diss.}}(t; p_T)}{dp_T} \right) = \frac{1}{t_{\text{diss.}}} \frac{d\sigma^{\text{meson}}(t; p_T)}{dp_T}. \quad (13)$$

Here we denote by $d\sigma^{Q\bar{Q}}(t; p_T)/dp_T$ the cross section to produce the proto-quarkonium states that evolve into an interacting with the medium meson on the time scale of $t_{\text{form.}}$. This time scale for the heavy quarks to interact with the QGP is taken in the relativistic limit. The initial condition at $t \approx 0$ includes the short distance perturbative $Q\bar{Q}$ production cross sections and the long-distance matrix elements for the particular quarkonium state. $d\sigma^{\text{meson}}(t; p_T)dp_T$ is the cross section for that quarkonium state as a function of time t . Finally, $d\sigma^{\text{diss.}}(t; p_T)/dp_T$ is the cross section of the dissociated $Q\bar{Q}$ pairs that will not produce quarkonia. In the absence of a medium $t_{\text{diss.}} \rightarrow \infty$ and the proto-quarkonium states evolve into the corresponding meson with unit probability. The system of equations Eqs. (12)-(13) has to be

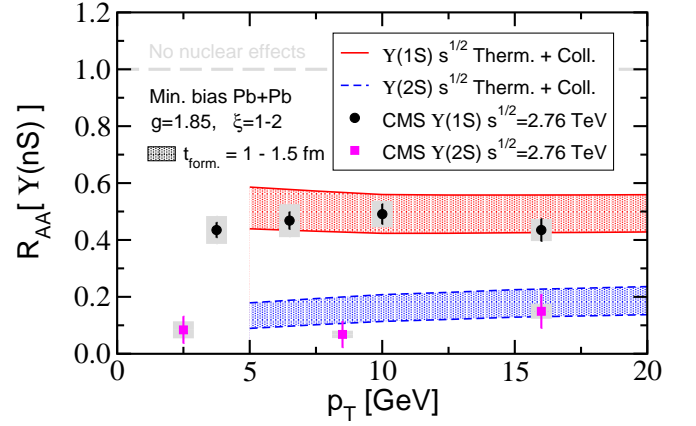


FIG. 4: (Color online) Comparison of theoretical results for the $\Upsilon(nS)$ R_{AA} in 2.76 TeV minimum bias Pb+Pb collisions versus p_T to CMS experimental measurements [39].

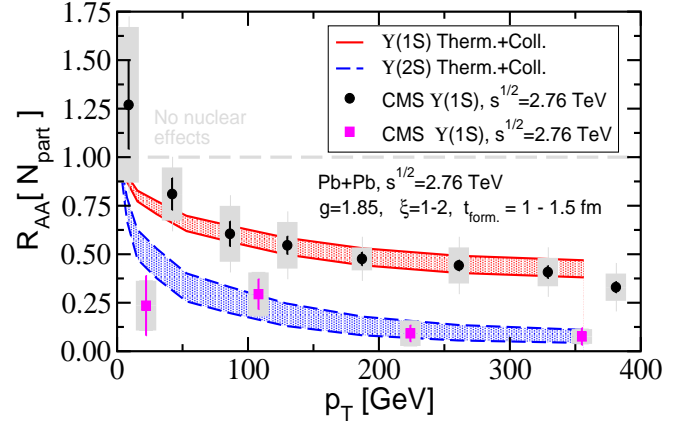


FIG. 5: (Color online) Suppression of $\Upsilon(1S)$, $\Upsilon(2S)$ in Pb+Pb collisions at 2.76 TeV is shown versus the number of participants for $p_T = 5$ GeV. Superimposed are CMS experimental data [39] on bottomonia suppression versus centrality.

solved for each of the quarkonium states listed in Table I. Feed-down is then performed using the NRQCD cross sections and branching ratios.

We start by first discussing results at the lower energy of $\sqrt{s} = 2.76$ TeV. In Fig. 3 we present the centrality dependence of prompt J/ψ s in Pb+Pb collisions. The bands reflect the combined uncertainty of the interaction onset time $t_{\text{form.}}$ and the collisional dissociation of the quarkonium states. In the evaluation of the latter we keep the coupling between the heavy quarks and the medium fixed at $g = 1.85$ [32] but vary the broadening parameter ξ . The upper edge of the uncertainty band corresponds to $t_{\text{form.}} = 1.5$ fm, $\xi = 1$. The lower edge of the uncertainty band corresponds to $t_{\text{form.}} = 1$ fm, $\xi = 2$. The upper panel of Fig. 3 shows comparison to the ALICE [35] and CMS [38] prompt J/ψ measurements. We find improved description in the most central N_{part} bins relative to the case when thermal screening effects were not included [32]. Around $N_{part} = 100$ the data lies on

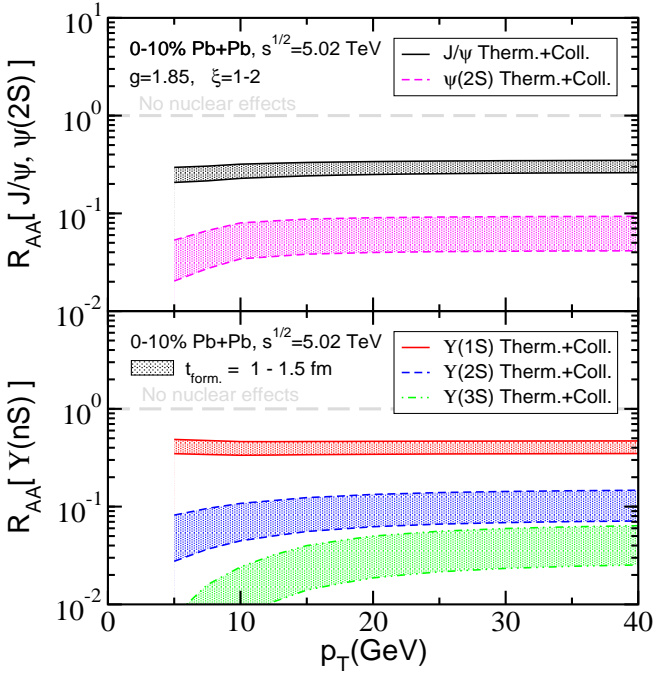


FIG. 6: (Color online) Theoretical model predictions for the R_{AA} of the ground and excited J/ψ (top panel) and Υ (bottom panel) states in 0-10% central Pb+Pb collisions at $\sqrt{s} = 5.02$ TeV at the LHC. The coupling between the heavy quarks and the medium $g = 1.85$ and the bands correspond to $t_{\text{form.}} = 1.5$ fm, $\xi = 1 - t_{\text{form.}} = 1$ fm, $\xi = 2$.

the upper edge of the theoretical error band. The bottom panel of Fig. 3 shows the J/ψ R_{CP} , where the 40%-80% peripheral collisions are used as a baseline. The ATLAS collaboration measured inclusive J/ψ [37]. However, in the $p_T < 10$ GeV interval which dominates the cross section, the non-prompt $B \rightarrow J/\psi$ contribution is limited to 20-30% [32] and will not noticeably affect the theoretical results.

Recently, experimental results for the differential suppression of the $\Upsilon(nS)$ family have appeared at high p_T [39]. Theoretical calculations for the $\Upsilon(1S)$ (red band) and $\Upsilon(2S)$ (blue band) in minimum bias $\sqrt{s} = 2.76$ TeV Pb+Pb reactions are shown in Fig. 4. We have evaluated the cross sections for quarkonia in 10 centrality classes (labeled i) and

$$R_{AA}^{\text{min. bias}}(p_T) = \frac{\sum_i R_{AA}((b_i)) W_i}{\sum_i W_i} \quad \text{where} \quad (14)$$

$$W_i = \int_{b_i^{\text{min}}}^{b_i^{\text{max}}} N_{\text{coll.}}(b) \pi b db.$$

The experimental data is described well, including its magnitude and p_T dependence. We note that collisional dissociation mostly affects the ground Υ state, while thermal wavefunction effects dominate the attenuation pattern of the excited Υ states. The CMS collaboration also put an upper limit on the $\Upsilon(3S)$ cross section in Pb+Pb reactions, corresponding to an upper limit on its

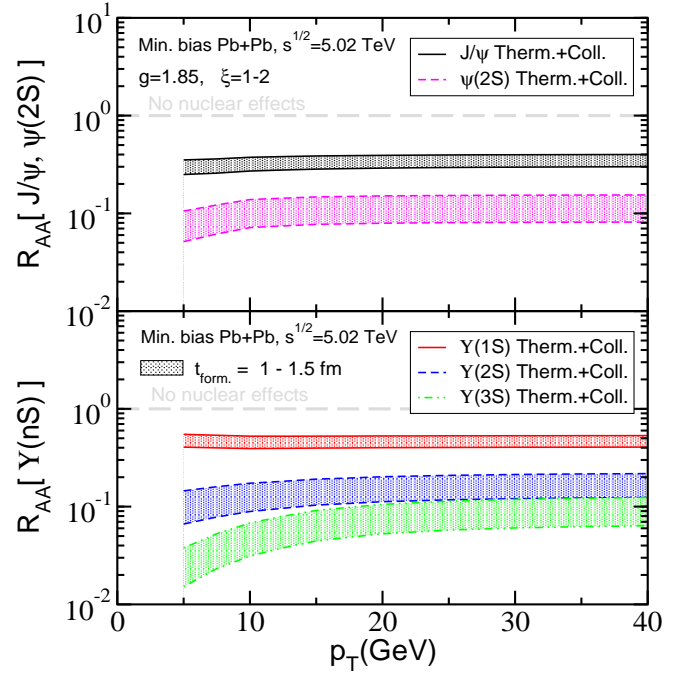


FIG. 7: (Color online) Same as in Fig. 6, but for minimum bias collisions.

R_{AA} [39]. Our calculated $\Upsilon(3S)$ cross section is consistent with this limit. While the theoretical approach presented in this Letter is applicable at large transverse momenta, we observe in Fig. 4 that the nuclear modification factor is approximately constant. This allows us to compare in Fig. 5 the centrality dependence in the lowest $p_T = 5$ GeV bin, not very different from the mean p_T of bottomonia at the LHC, to the experimentally measured $\Upsilon(1S)$ and $\Upsilon(2S)$ R_{AA} dependence on the number of participants [39]. Very good agreement between data and theory is observed.

In Figs. 6 and 7, we present theoretical predictions for the R_{AA} of various quarkonium species as a function of p_T in Pb+Pb collisions at $\sqrt{s} = 5.02$ TeV. The top and bottom panels display results for charmonium and bottomonium states, respectively. We find a clear separation in suppression based on how tightly bound the quarkonium state is. We also find a flat or slightly increasing R_{AA} with p_T . By comparing Fig. 6 to Fig. 7, we observe that the attenuation of quarkonia in minimum bias collisions is only slightly smaller than in the most central collisions. The reason for that behavior is that minimum bias collisions are strongly dominated by the first 3 most central classes, as given by the weights W_i in Eq. (14).

Very recently, at $\sqrt{s} = 5.02$ TeV, measurements of relative suppression ratios of excited to ground quarkonium states have appeared [40, 63]. The data for $\psi(2S)/J/\psi$ is publicly available and shown in Fig. 8. Theoretically, the double suppression ratio can be obtained from the results in Fig. 7 and is compatible with the experimental data within the statistical and systematic error bars.

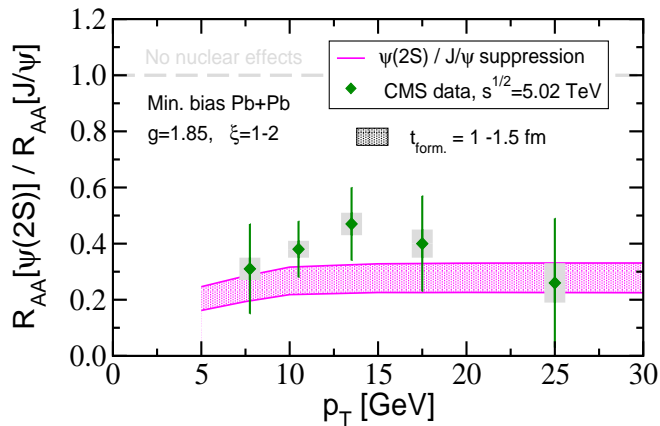


FIG. 8: (Color online) Theoretical model predictions for the double $(\psi(2S))_{AA}/(\psi(2S))_{pp}/(J/\psi)_{AA}/(J/\psi)_{pp}$ ratio in minimum bias Pb+Pb collisions at $\sqrt{s} = 2.76$ TeV at the LHC. Data is from CMS [40].

IV. CONCLUSIONS

In summary, we presented theoretical results for the p_T -differential suppression of charmonia and bottomonia in Pb+Pb collisions at the LHC. The dynamics of $Q\bar{Q}$ pairs, which evolve into the observed quarkonium states, is governed in HICs by the formation and dissociation time scales. A key element of our formalism that addresses this dynamics is that the formation time of proto-quarkonia is ~ 1 fm. We assume that this time scale is long enough that the $Q\bar{Q}$ interact via a color screened thermal potential [6, 9]. Therefore we employ the wavefunctions obtained by solving the Schrödinger equation for $Q\bar{Q}$ interacting via a screened potential to calculate the dissociation time scale, using the theoretical setup described in [32]. The technical advances that are further incorporated in the calculation are better constraints on the NRQCD matrix elements that are relevant for the production of high- p_T $\psi(2S)$ and χ_c states, and their feed-down to J/ψ , and 2+1 dimensional event-by-event hydrodynamic modeling of the QGP background [33].

We explored the phenomenological implications of this theoretical model for quarkonium production and propagation in the QGP background created in heavy ion collisions, first around mid-rapidity in Pb+Pb collisions at the LHC. We found good separation in the magnitude of the suppression between the ground and excited charmonium and bottomonium states, compatible with recent experimental measurements. Our results indicate that effects of thermal screening of the $Q\bar{Q}$ attractive potential fully dominate the attenuation of $\psi(2S)$, $\Upsilon(2S)$ and $\Upsilon(3S)$. On the other hand, J/ψ and $\Upsilon(1S)$ are also sensitive to the dissociation processes due to collisional interactions. The approximately constant or slightly decreasing R_{AA} with p_T predicted by this model arises from the early $\mathcal{O}(1$ fm) formation of the interacting quarkonium state. The uncertainty of the phenomenological results was estimated by varying the formation time and the strength of the collisional broadening of the $Q\bar{Q}$ pair. We found that the charmonium suppression measurements are better described by the upper edge of the R_{AA} uncertainty band, whereas bottomonium suppression measurements are better described by its lower edge. While an illustrative subset of results was presented here, detailed predictions are available that will allow to test this model versus upcoming experimental measurements of quarkonium suppression at $\sqrt{s} = 5.02$ TeV.

In the future, we plan to address data at finite rapidity with the same parameters and test the model further. This will likely require inclusion of CNM effects since p -Pb data at finite rapidity seems to show non-trivial nuclear modification patterns. It will also be interesting and instructive to investigate non-prompt J/ψ production, which probes the complementary but different physics of in-medium modification of heavy-quark parton showers [64, 65].

Acknowledgments: This research is supported by the US Department of Energy, Office of Science, under Contract No. DE-AC52-06NA25396 and in part by the DOE Early Career Program. We are grateful to C. Shen for help with the iEBE-VISHNU code. RS thanks J. P. Blaizot, S. Datta, R. Gavai, S. Gupta, and A. Tiwari for rewarding discussions on the topic.

-
- [1] A. Mocsy, P. Petreczky, and M. Strickland, Int. J. Mod. Phys. **A28**, 1340012 (2013), 1302.2180.
[2] S. Datta, Pramana **84**, 881 (2015), 1403.8151.
[3] A. Andronic et al., Eur. Phys. J. **C76**, 107 (2016), 1506.03981.
[4] T. Matsui and H. Satz, Phys. Lett. **B178**, 416 (1986).
[5] X.-M. Xu, D. Kharzeev, H. Satz, and X.-N. Wang, Phys. Rev. **C53**, 3051 (1996), hep-ph/9511331.
[6] O. Kaczmarek and F. Zantow, Phys. Rev. **D71**, 114510 (2005), hep-lat/0503017.
[7] A. Bazavov and P. Petreczky, Nucl. Phys. **A904-905**, 599c (2013), 1210.6314.
[8] Y. Burnier, O. Kaczmarek, and, A. Rothkopf, JHEP **1512**, 101 (2015) 1509.07366.
[9] A. Mocsy and P. Petreczky, Phys. Rev. Lett. **99**, 211602 (2007), 0706.2183.
[10] M. Laine, O. Philipsen, P. Romatschke, and M. Tassler, JHEP **03**, 054 (2007), hep-ph/0611300.
[11] M. Margotta, K. McCarty, C. McGahan, M. Strickland, and D. Yager-Elorriaga, Phys. Rev. **D83**, 105019 (2011), [Erratum: Phys. Rev.D84,069902(2011)], 1101.4651.
[12] N. Brambilla, M. A. Escobedo, J. Ghiglieri, and A. Vairo,

- JHEP **05**, 130 (2013), 1303.6097.
- [13] M. A. Escobedo, F. Giannuzzi, M. Mannarelli, and J. Soto, Phys. Rev. **D 87**, 114005 (2013) 1304.4087.
- [14] P. Petreczky, C. Miao, and, A. Mocsy, Nucl. Phys. **A 855**, 125 (2011) 1012.4433.
- [15] A. Rothkopf, T. Hatsuda, and, S. Sasaki, PoS LAT **162** (2009) 0910.2321.
- [16] M. Strickland, Phys. Rev. Lett. **107**, 132301 (2011), 1106.2571.
- [17] T. Song, Phys. Rev. **C89**, 044903 (2014), 1402.3451.
- [18] J. Hoelck, F. Nendzig, and G. Wolschin, Phys. Rev. **C95**, 024905 (2017), 1602.00019.
- [19] B. Krouppa, R. Ryblewski, and M. Strickland, Phys. Rev. **C92**, 061901 (2015), 1507.03951.
- [20] Y. Akamatsu and A. Rothkopf, Phys. Rev. **D85**, 105011 (2012), 1110.1203.
- [21] J.-P. Blaizot, D. De Boni, P. Faccioli, and G. Garberoglio, Nucl. Phys. **A946**, 49 (2016), 1503.03857.
- [22] N. Brambilla, M. A. Escobedo, J. Soto, and A. Vairo, Phys. Rev. **D96**, 034021 (2017), 1612.07248.
- [23] S. Kajimoto, Y. Akamatsu, M. Asakawa, and A. Rothkopf (2017), 1705.03365.
- [24] F. Riek, and, R. Rapp, New J. Phys. **13**, 045007 (2011) 1012.0019.
- [25] F. Riek and R. Rapp, Phys. Rev. C **82**, 035201 (2010) 1005.0769
- [26] R. Rapp and H. van Hees, in Quark-gluon plasma 4 (2010), pp. 111–206, 0903.1096.
- [27] A. Emerick, X. Zhao, and R. Rapp, Eur. Phys. J. **A48**, 72 (2012), 1111.6537.
- [28] X. Du, R. Rapp, and M. He (2017), 1706.08670.
- [29] J. Casalderrey-Solana, H. Liu, D. Mateos, K. Rajagopal, and U. A. Wiedemann (2011), 1101.0618.
- [30] A. Adil and I. Vitev, Phys. Lett. **B649**, 139 (2007), hep-ph/0611109.
- [31] R. Sharma, I. Vitev, and B.-W. Zhang, Phys. Rev. **C80**, 054902 (2009), 0904.0032.
- [32] R. Sharma and I. Vitev, Phys. Rev. **C87**, 044905 (2013), 1203.0329.
- [33] C. Shen, Z. Qiu, H. Song, J. Bernhard, S. Bass, and U. Heinz, Comput. Phys. Commun. **199**, 61 (2016), 1409.8164.
- [34] G. T. Bodwin, E. Braaten, and G. P. Lepage, Phys. Rev. **D51**, 1125 (1995), [Erratum: Phys. Rev. **D55**, 5853(1997)], hep-ph/9407339.
- [35] J. Adam et al. (ALICE), JHEP **07**, 051 (2015), 1504.07151.
- [36] B. B. Abelev et al. (ALICE), Phys. Lett. **B734**, 314 (2014), 1311.0214.
- [37] G. Aad et al. (ATLAS), Phys. Lett. **B697**, 294 (2011), 1012.5419.
- [38] V. Khachatryan et al. (CMS), Eur. Phys. J. **C77**, 252 (2017), 1610.00613.
- [39] V. Khachatryan et al. (CMS), Phys. Lett. **B770**, 357 (2017), 1611.01510.
- [40] A. M. Sirunyan et al. (CMS), Phys. Rev. Lett. **118**, 162301 (2017), 1611.01438.
- [41] P. L. Cho and A. K. Leibovich, Phys. Rev. **D53**, 150 (1996), hep-ph/9505329.
- [42] E. Braaten, S. Fleming, and A. K. Leibovich, Phys. Rev. **D63**, 094006 (2001), hep-ph/0008091.
- [43] M. Butenschoen and B. A. Kniehl, Phys. Rev. **D84**, 051501 (2011), 1105.0820.
- [44] K. Wang, Y.-Q. Ma, and K.-T. Chao, Phys. Rev. **D85**, 114003 (2012), 1202.6012.
- [45] G. T. Bodwin, H. S. Chung, U.-R. Kim, and J. Lee, Phys. Rev. Lett. **113**, 022001 (2014), 1403.3612.
- [46] M. Baumgart, A. K. Leibovich, T. Mehen, and I. Z. Rothstein, JHEP **11**, 003 (2014), 1406.2295.
- [47] Z.-B. Kang, J.-W. Qiu, F. Ringer, H. Xing, and H. Zhang, Phys. Rev. Lett. **119**, 032001 (2017), 1702.03287.
- [48] R. Bain, L. Dai, A. Leibovich, Y. Makris, and T. Mehen, Phys. Rev. Lett. **119**, 032002 (2017), 1702.05525.
- [49] R. Aaij et al. (LHCb), Phys. Rev. Lett. **118**, 192001 (2017), 1701.05116.
- [50] B. Schenke, S. Jeon, and C. Gale, Phys. Rev. **C82**, 014903 (2010), 1004.1408.
- [51] M. Habich, J. L. Nagle, and P. Romatschke, Eur. Phys. J. **C75**, 15 (2015), 1409.0040.
- [52] M. Gyulassy, P. Levai, and I. Vitev, Phys. Rev. **D66**, 014005 (2002), nucl-th/0201078.
- [53] R. L. Thews, Nucl. Phys. **A783**, 301 (2007), hep-ph/0609121.
- [54] S. Gupta and R. Sharma, Phys. Rev. **C89**, 057901 (2014), 1401.2930.
- [55] J.-w. Qiu and I. Vitev, Phys. Lett. **B570**, 161 (2003), nucl-th/0306039.
- [56] J.-W. Qiu and I. Vitev, Phys. Lett. **B587**, 52 (2004), hep-ph/0401062.
- [57] I. Vitev, J. T. Goldman, M. B. Johnson, and J. W. Qiu, Phys. Rev. **D74**, 054010 (2006), hep-ph/0605200.
- [58] Z.-B. Kang, I. Vitev, and H. Xing, Phys. Rev. **C92**, 054911 (2015), 1507.05987.
- [59] R. Vogt, Phys. Rev. **C92**, 034909 (2015), 1507.04418.
- [60] J. Adam et al. (ALICE), JHEP **06**, 055 (2015), 1503.07179.
- [61] A. M. Sirunyan et al. (CMS), Eur. Phys. J. **C77**, 269 (2017), 1702.01462.
- [62] M. Aaboud et al. (ATLAS) (2017), 1709.03089.
- [63] A. M. Sirunyan et al. (CMS) (2017), 1706.05984.
- [64] Z.-B. Kang, F. Ringer, and I. Vitev, JHEP **03**, 146 (2017), 1610.02043.
- [65] J. Huang, Z.-B. Kang, and I. Vitev, Phys. Lett. **B726**, 251 (2013), 1306.0909.